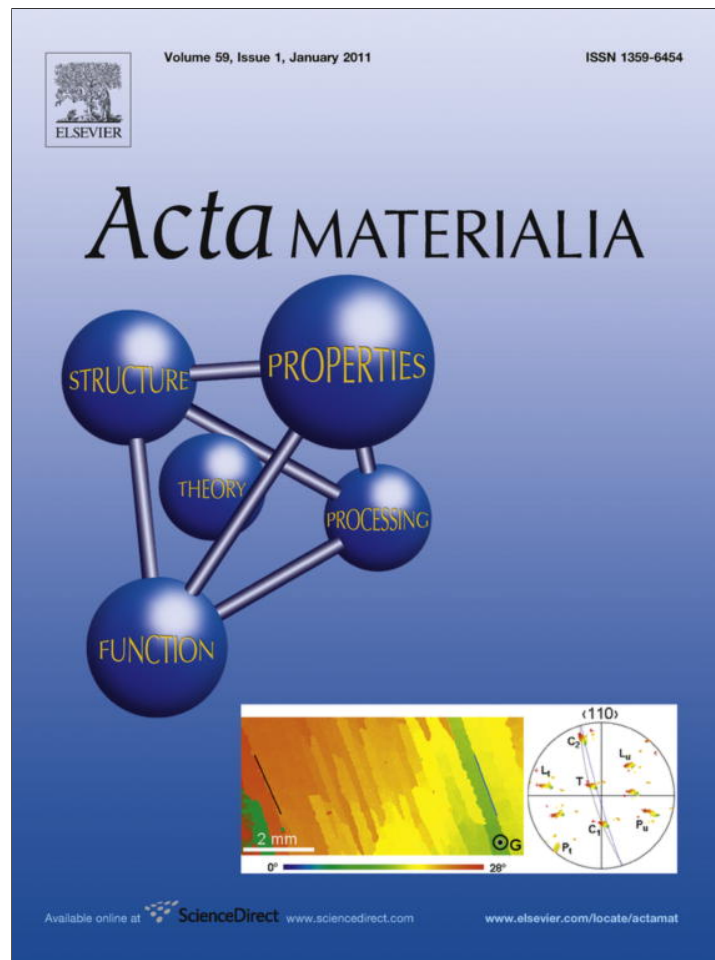


Provided for non-commercial research and education use.
Not for reproduction, distribution or commercial use.



(This is a sample cover image for this issue. The actual cover is not yet available at this time.)

This article appeared in a journal published by Elsevier. The attached copy is furnished to the author for internal non-commercial research and education use, including for instruction at the authors institution and sharing with colleagues.

Other uses, including reproduction and distribution, or selling or licensing copies, or posting to personal, institutional or third party websites are prohibited.

In most cases authors are permitted to post their version of the article (e.g. in Word or Tex form) to their personal website or institutional repository. Authors requiring further information regarding Elsevier's archiving and manuscript policies are encouraged to visit:

<http://www.elsevier.com/copyright>



On the specific surface area of nanoporous materials

E. Detsi^a, E. De Jong^a, A. Zinchenko^a, Z. Vuković^b, I. Vuković^c, S. Punzhin^a, K. Loos^c,
G. ten Brinke^c, H.A. De Raedt^a, P.R. Onck^a, J.T.M. De Hosson^{a,*}

^a Department of Applied Physics, Zernike Institute for Advanced Materials and Materials Innovation Institute, University of Groningen, Nijenborgh 4, 9747 AG Groningen, The Netherlands

^b Institute of Chemistry Technology and Metallurgy, Department of Catalysis and Chemical Engineering, Njegoševa 12, 11000 Belgrade, Serbia

^c Physical Chemistry of Polymers, Zernike Institute for Advanced Materials, University of Groningen, Nijenborgh 4, 9747 AG Groningen, The Netherlands

Received 3 May 2011; received in revised form 12 July 2011; accepted 18 August 2011

Abstract

A proper quantification of the specific surface area of nanoporous materials is necessary for a better understanding of the properties that are affected by the high surface-area-to-volume ratio of nanoporous metals, nanoporous polymers and nanoporous ceramics. In this paper we derive an analytical expression that relates the specific surface area of arbitrary nanoporous materials to their solid bulk density and ligament size. Computed specific surface areas of porous materials with regular nanopores are in good agreement with the expression derived. These regular void geometries include single and double gyroid structures, as well as materials with spherical and cylindrical nanopores. Validation of the expression for disordered nanoporous materials is performed by investigation of the specific surface areas of various nanoporous gold electrodes in the double-layer charging regime.

© 2011 Acta Materialia Inc. Published by Elsevier Ltd. All rights reserved.

Keywords: Specific surface area; Nanoporous materials; Catalysts; Sensors; Actuators

1. Introduction

When the length scale of a material decreases from macro to nano, the fraction of surface atoms with respect to the bulk increases and this may substantially affect the physical properties depending on the surface state. Material properties associated with the high surface-area-to-volume ratio are relevant for various applications, including catalysts [1–3], electrochemical supercapacitors [4,5], sensors and electrochemical actuators [6–9]. In particular, nanoporous metallic materials are very promising as actuation materials, because they are susceptible to producing large strain in combination with high stiffness and strength, in contrast to polymer actuation materials, which generate large strain but with low stiffness and strength; or to piezoceramic materials, which are stiff and strong but

with restricted strain amplitudes [7]. Qualitatively, macroscopic dimensional changes observed in nanoporous gold are associated with changes in surface stress.

In all these applications, nanoporous materials are usually quantified with respect to their structure sizes, weight or volume, rather than their specific surface area. This is mainly because of the lack of an efficient method to quantify the specific surface area of these materials, based on their ligament and pore size. The specific surface area of nanoporous materials with regular pore geometries can be calculated from well-defined unit cells. However, commonly used nanoporous materials display a disordered structure characterized by randomly oriented nanoscale features, therefore an exact analytical evaluation of their specific surface area is impossible.

A well-recognized approach to determine the specific surface area of nanoporous materials is the Brunauer, Emmett and Teller (BET) method [10–14], which is based on physical adsorption of gas molecules to determine the specific surface area. Although this method is very reliable, it is not always

* Corresponding author. Tel.: +31 50 3634898; fax: +31 50 3634881.
E-mail address: j.t.m.de.hosson@rug.nl (J.T.M. De Hosson).

accessible for routine checks on specific surface areas, e.g. for commonly used setups (e.g. Sorptomatic 1990 Thermo Finnigen); at least a few hundred milligrams of porous material is required for a reliable specific surface area evaluation. In the case of nanoporous gold, this amount is excessive, compared to the few milligrams of a sample required for common experiments on nanoporous metals [1,4,6–9,15]. For this reason material properties associated with the specific surface area are usually described with respect to their weight or volume, rather than their specific surface area.

This paper is aimed at filling this gap by investigating a model based on the size of the nanoscale features of nanoporous materials and their solid bulk densities. Analytic, computational and experimental approaches were employed to derive and validate this model, as follows.

- (i) From dimensional analysis, a general relationship for the specific surface area of any arbitrary nanoporous material was derived. The expression depends on the solid bulk density of the material, and on the size of the ligaments or pores. The expression contains an unknown dimensionless constant which can be computed for nanoporous materials with regular and periodic voids.
- (ii) The validity of the derived relationship was investigated by comparing its outcome with the computed specific surface areas for nanoporous materials with pores having a regular and periodic geometry. From these computations, the unknown dimensionless constant mentioned in (i) was determined in the cases of single and double gyroid structures, as well as spherical and cylindrical voids.
- (iii) For disordered nanoporous materials, the aforementioned constant has been experimentally determined by investigating the specific surface area of a set of eight nanoporous gold samples having different average ligament sizes and porous bulk densities. The specific surface areas obtained from electrochemical measurements are compared with the results from BET analysis.

2. Analytic and computational methods

2.1. Derivation

Dimensional analysis is a powerful method to investigate the relation between physical quantities by comparing their dimensions [16]. Let S represent the specific surface area of an arbitrary nanoporous material. From dimensional considerations, S can be expressed as a function of some variables x_1, x_2, \dots, x_n , as follows:

$$S = f(x_1, x_2, \dots, x_n) \quad (1)$$

Dimensional analysis exploits the fact that both quantities S and $f(x_1, x_2, \dots, x_n)$ in Eq. (1) have the same dimension. The variables x_1, x_2, \dots, x_n represent basic physical

parameters associated with the physical quantity S . By definition, the specific surface area of a material is the ratio of its surface area to its mass. Therefore basic physical parameters associated with the specific surface area of an arbitrary nanoporous material includes: (i) its intrinsic size (ligament and pore size), which carries necessary information about the surface area of the nanoscale features, and (ii) the porous bulk density of the material, which carries necessary information about the weight and volume of the material. If ρ^* and d represent the porous bulk density of the nanoporous material and its ligament size (assuming ligament and pore sizes are comparable), respectively, then Eq. (1) becomes:

$$S = f(\rho^*, d) \quad (2)$$

According to Buckingham's pi theorem, the number of dimensionless groups associated with Eq. (2) is given by the difference between the number of parameters and the number of physical dimensions involved. Eq. (2) displays three parameters (S, ρ^*, d) and two basic physical dimensions (meters, grams), which means that only one dimensionless group can be derived from Eq. (2). Derivation of this dimensionless group gives the following dimensionless constant that we denote C^* (see Appendix A for details): $S\rho^*d = C^*$; from this, the dependence of the specific surface area S on the porous bulk density ρ^* and the ligament size d can be deduced:

$$S = \frac{C^*}{\rho^*d} \quad (3)$$

By replacing the porous bulk density ρ^* in Eq. (3) by the product $\rho_r\rho$, where ρ_r and ρ are the relative and solid bulk densities, Eq. (3) becomes:

$$S = \frac{C}{\rho d} \quad (4)$$

with $C = C^*/\rho_r$. Eq. (4) can be exploited to evaluate the specific surface area of any arbitrary nanoporous material, knowing its solid bulk density and ligament size, provided that the dimensionless constant is determined. It should be emphasized that ρ in Eq. (4) represents the solid bulk density rather than the porous bulk density. Indeed, the derivation of Eq. (4) is based on the assumption that the ligament and pore sizes are comparable, which automatically means that the material porous bulk density is fixed. In practice, the relative density (or porous bulk density) may vary but variations in the relative density for a given type of nanoporous material are usually restricted to a small range. In the case of nanoporous gold, the investigated relative densities in literature usually vary between $\sim 20\%$ and $\sim 35\%$ [15]. We will show in the experimental section that these small variations in the value of the relative density do not significantly affect the value of the specific surface area S as given in Eq. (4): e.g. for nanoporous gold the difference in the specific surface area between two samples with the same average ligament size d , but with different relative densities (25% and 30%) was found to be less than 10%, which is within the error bars.

Computed specific surface areas based on unit cells displayed in Fig. 1a and b are found to increase (or decrease) by about 20%, when the ratio of the ligament diameter to the pore size is lowered from 1 to 0.8 (or augmented from unity to ~ 1.2). Indeed, if the ratio of the ligament diameter to the pore size is less than ~ 0.8 or higher than ~ 1.2 , the predicted specific surface areas from Eq. (4) become less accurate. In that case, if d_ℓ and d_p represent the size of the ligaments and pores, respectively, then Eq. (1) will give rise to four parameters (S , ρ^* , d_ℓ , d_p) and two basic physical dimensions (meters, grams). Following Buckingham's pi theorem this will result in an expression with two dimensionless groups, which can be derived from dimensional considerations:

$$S = \frac{C}{\rho d_\ell} \times \left(\frac{d_\ell}{d_p}\right)^\alpha \quad (5)$$

In Eq. (5), ρ represents the solid bulk density introduced in a similar way as in Eq. (4). The exponent α represents an additional unknown constant. Note that the factor $\left(\frac{d_\ell}{d_p}\right)^\alpha$ is a measure for the porous bulk density [17], which means that when the ratio of ligament diameter to pore size is no longer fixed, the porous bulk density can no longer be assumed constant as in Eq. (4).

In this paper, we focus on Eq. (4), where ligament and pore sizes are comparable, and it should be valid for any arbitrary nanoporous material. In order to verify this for materials with regular pore geometries, and also to get more insight on the nature of the dimensionless constant, we consider a simple case of a cubic porous bulk material with external dimensions L^3 (volume). Assuming for simplicity that the pores are unidirectional cylinders, all having a diameter d , the specific surface area (S_{cube}) of such a porous material can be cast into an analytical expression. The specific surface area of the porous cube does not depend on the dimension (L^3) of the cube nor the number of cylinders in the cube. S_{cube} depends rather on the material solid bulk density ρ and on the cylinder diameter d , in agreement with Eq. (4). (The derivation is detailed in Appendix B.)

By comparing Eq. (4) and Eq. (A22) from Appendix B, it is obvious that C in Eq. (4) corresponds to the dimensionless factor $\frac{4(1-\rho_r)}{\rho_r}$ from Eq. (A22). Clearly, it depends on the nanoporous material relative density and on a factor associated with the type of porous geometry taken into consideration (e.g. cylindrical or spherical pores, gyroid structures and disordered nanoporous materials). For a given porous geometry and relative density, C in Eq. (4) is constant as required by the dimensional analysis. In

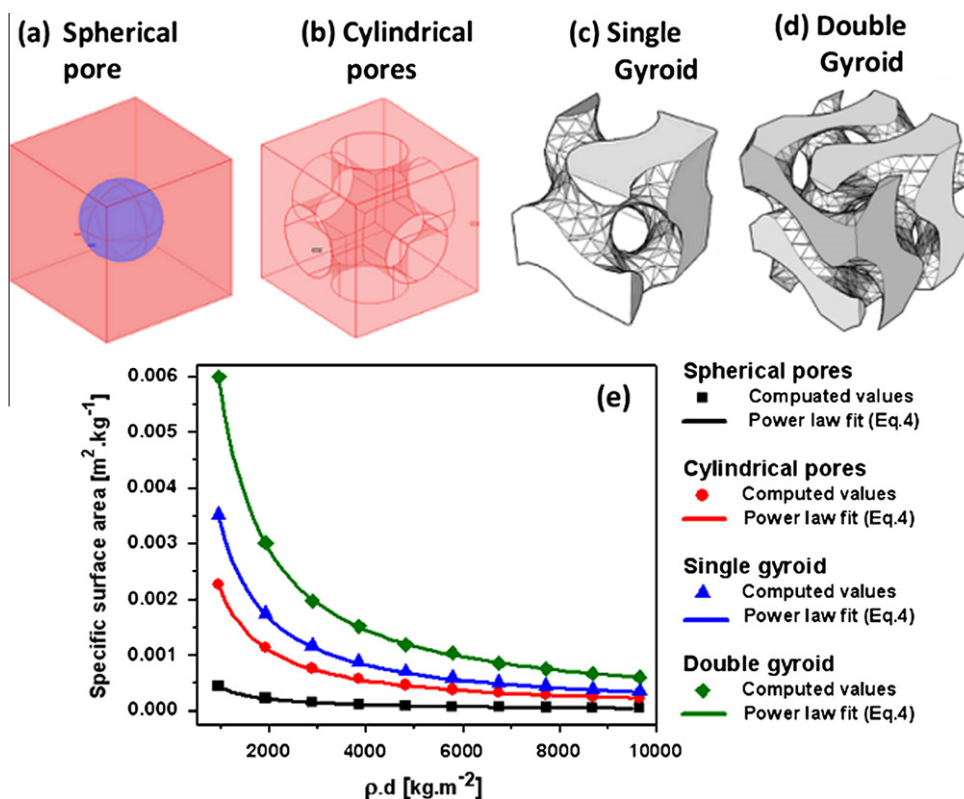


Fig. 1. Comparison between computed specific surface areas of nanoporous materials with regular and periodic voids and those predicted from Eq. (4). Four types of regular structures are investigated: (a) spherical voids, (b) cylindrical voids, (c) single gyroid and (d) double gyroid structures. (e) For each type of structure, computed values for its specific surface area (black squares, red circles, blue triangles and green rhombus) are in good agreement with predictions from the derived model (black, red, blue and green lines). (For interpretation of the references to colour in this figure legend, the reader is referred to the web version of this article.)

order to explore Eq. (4) for the determination of the specific surface area of any arbitrary material, the value of the dimensionless constant for that specific porous material is required. In the next section, values of this constant are derived for commonly encountered porous structures.

2.2. Regular and periodic pore geometries

The validity of the expression derived in Eq. (4) was further investigated by comparing its outcome with computed specific surface areas of nanoporous materials having regular and periodic pore geometries. Four types of geometries were investigated: spherical and cylindrical voids, and single and double gyroid structures. The unit cells used for these computations are displayed in Fig. 1a–d. The finite element analysis simulation software COMSOL Multiphysics was employed to evaluate the specific surface area for each of the four geometries. For each type of geometry in Fig. 1a–d, the size of the ligament was tuned at constant porous bulk density ρ^* by simply varying the size of the unit cell: when the size of a unit cell increases, the corresponding ligaments size increases as well, but ρ^* remains constant. Investigated relative densities for each type of porous geometry are found in Table 1. COMSOL Multiphysics can evaluate the total surface area and volume of an object (unit cell). From these total surface area and volume, the specific surface area can be deduced, knowing the porous bulk density of the object. Ten different ligament sizes were investigated for each type of unit cell in Fig. 1a–d. The outcomes are displayed by solid markers (black squares, red circles, blue triangles and green rhombus) in Fig. 1e.

Eq. (4) denotes that the specific surface area (S) of an arbitrary unit cell depends on the size of the ligament (d) and the solid bulk density (ρ) of the material. If ρ^* is maintained constant as aforementioned, the specific surface area will only depend on the ligament diameter (d). According to Eq. (4) the specific surface area S is inversely proportional to ρd . To verify this, we plot the aforementioned computed values of S as a function of ρd . For each type of unit cell, the best fits (the solid lines in Fig. 1e) associated

to the computed data (the solid markers in Fig. 1e) are indeed inversely proportional to ρd . This means that Eq. (4) can be used to determine the specific surface area of nanoporous materials with regular and periodic pores for a specific relative density, provided that the value of the constant in this equation is known. Knowing the solid bulk density (ρ) and the corresponding ligament size d in each unit cell, the dimensionless constant can be deduced for each type of unit cell shown in Fig. 1e, by comparing the best fits with Eq. (4). As previously mentioned, this constant is observed to vary with the type of pore geometry taken into consideration. The value of this constant was found to be ~ 0.4 for spherical pores, ~ 2.7 for cylindrical pores with one cylinder per unit cell, ~ 2.1 for cylindrical pores with two crossing cylinders per unit cell, ~ 3.4 for single gyroid and ~ 5.8 for double gyroid structures. These values for the investigated relative densities are summarized in Table 1.

The BET surface area of periodic nanoporous polymers having a double gyroid structure, formed by self-assembly of block copolymer-based supramolecular complexes will be evaluated and compared to the double gyroid specific surface area using Eq. (4) in the next section.

3. Experimental procedures

3.1. Motivation and methods

Translational invariant unit cells in disordered nanoporous materials are not properly defined due to the random shapes of the ligaments and voids in these materials. Therefore, computation of the specific surface area as in the previous section is not straightforward. The validity of Eq. (4) for disordered nanoporous materials was therefore scrutinized by an experimental approach aimed at evaluating the specific surface areas S of a set of eight nanoporous gold samples with different ligament sizes d and porous bulk density ρ^* and plotting the values of S as a function of ρd . In principle the BET method is an ideal experimental tool for the investigation of these surface areas; however for each BET measurement (i.e. each ligament size), at least 250 mg of nanoporous gold is required for reliable results. In total it corresponds to a total of 2 g of nanoporous gold for the eight different ligament sizes investigated. Note that about 4 g of silver is needed in order to synthesize 2 g of nanoporous gold by dealloying an Au–Ag binary system, representing a considerable amount of noble metals because only a few milligrams of material are commonly used for experiments on nanoporous metals [1,4,6–9,15]. As a consequence, rather than the BET method, an alternative approach was explored in order to investigate experimentally the specific surface area of the set of eight nanoporous Au samples.

In the BET method, the amount of gas sufficient to form a monolayer adsorbed onto a porous material at low relative pressures is used to determine the surface area. Similarly, the concentration of ions adsorbed on an electrode

Table 1

The various geometries and relative densities are listed in the 1st and 2nd column, respectively. The corresponding value of the dimensionless constant (Eq. (4)) is listed in the 3rd column.

Nanostructures	Investigated relative densities (%)	Dimensionless constant
Spherical pores	93	0.4
Cylindrical pores (one cylinder/unit cell)	59	2.7
Cylindrical pores (two crossing cylinders/unit cell)	60	2.1
Single gyroid	46	3.4
Double gyroid	51 and 57	5.8
Disordered nanoporous structures	10, 15, 25 and 30	3.7

can provide information on the electrode surface area: the electrochemical behavior of a gold electrode in an acid environment is characterized by a double layer charging regime where oxygen species (OH^- , O_2^-) are reversibly electro-adsorbed onto the gold surface [18,19]. The electric charge transferred during the adsorption of these anions was used as a measure to investigate the variation of the specific surface areas of our nanoporous gold samples with respect to Eq. (4). This electrochemical approach is suitable for investigating the validity of Eq. (4) because one is not interested in the absolute values of the specific surface areas of the gold samples, but rather in the general dependence of the specific surface areas on the ligament size and solid bulk density. If this dependence is in agreement with Eq. (4), then one BET measurement is enough to evaluate the exact value of the dimensionless constant in Eq. (4) for disordered nanoporous materials. It appears that a combination of electrochemical and BET measurements is rather efficient because for all eight electrochemical measurements 80 mg of nanoporous gold is sufficient, whereas 2 g of material would be required for the BET method.

The electrochemical method used to investigate the validity of Eq. (4) assumes that the quantity of electric charge adsorbed onto a gold surface in the double layer charging regime is proportional to the gold electrode surface area. Prior to extending this hypothesis to nanoporous gold samples with unknown surface areas, this assumption was first verified on a set of seven planar solid gold films with known surface areas.

During investigations of the specific surface areas for both planar solid and nanoporous gold electrodes, cyclic voltammeteries were performed in 1 M perchloric acid in the potential range between 0.55 and 0.75 V with respect to an Ag/AgCl reference electrode. These voltammetry experiments were carried out at room temperature, at a scan rate of 20 mV s^{-1} using a potentiostat ($\mu\text{Autolab III-FRA2}$, Eco Chemie).

3.2. Materials: nanoporous metals and nanoporous polymers

Three different materials were investigated: (i) nanoporous polymers with a double gyroid structure used for BET measurements in order to verify the value of the dimensionless constant computed in Section 2.2 for double gyroid structures; (ii) planar solid gold foils with known surface areas, used for electrochemical measurements to verify the dependence on the adsorbent surface area of the quantity of electric charge transferred during electro-adsorption; (iii) nanoporous gold samples with different ligament sizes and porous bulk densities, and with unknown surface areas, used for electrochemical measurements in order to investigate the validity of Eq. (4). Nanoporous gold samples were further used for BET measurements, to determine the value of the constant in Eq. (4) for disordered nanoporous materials.

Nanoporous polymer was obtained from the supramolecular complex PS-b-P4VP (PDP) by selective PDP disso-

lution in ethanol. Films of the supramolecular complex with gyroid morphology were cast by dissolving the diblock copolymer of polystyrene and poly(4-vinylpyridine) (PS-b-P4VP, Polymer Source Inc.) and 3-pentadecylphenol (PDP, Aldrich 98 wt.% purity) in chloroform, followed by solvent annealing in a saturated chloroform atmosphere. For specific details we refer to Refs. [20–24].

In total seven planar solid gold foils with an average thickness of 20 μm , having surface areas of 20, 42, 62, 75, 95, 118 and 138 cm^2 were used as working electrodes. These gold foils were obtained by cold-rolling of pure gold (99.99%, Thessco BV, NL) followed by polishing with silicon carbide paper (FEPA P #2400, Struers) and cleaning in ultrasonic baths (acetone and demineralized water). Similar planar solid gold foils were used as counter electrodes.

Eight nanoporous gold samples were made by dealloying gold–silver alloys with composition $\text{Au}_{10}\text{Ag}_{90}$, $\text{Au}_{15}\text{Ag}_{85}$, $\text{Au}_{25}\text{Ag}_{75}$ (at.%). The master alloy for each composition was prepared by arc melting of pure gold (99.99%) and silver (99.999%, Thessco BV, NL) followed by homogenization in quartz tubes at 950 $^\circ\text{C}$ for 56 h. Rectangular blocks with dimensions $2 \times 1 \times 1 \text{ mm}^3$ were cut from these master alloys by spark erosion and sealed again in quartz tubes for annealing at 850 $^\circ\text{C}$ for 3 h. Silver was selectively removed from the alloys [1,4,7–9,15,25,26] by free corrosion in 65% HNO_3 – a process known as dealloying. In order to achieve a wide range of ligament sizes, some of the dealloyed samples were kept in acid for coarsening or subjected to post-annealing treatments (20 min at 200 $^\circ\text{C}$ and 30 min at 300 $^\circ\text{C}$). Electrochemical cleaning (repeated cathodic scans) was carried out to reduce the gold oxide layer formed during the free corrosion process [27]. These nanoporous gold samples were used as working electrodes for the investigation of their specific surface area during electro-adsorption of anions in the double layer charging region. Similar nanoporous gold samples were used as counter electrodes.

In addition to the aforementioned nanoporous gold samples, a 500 mg Au–Ag alloy with composition $\text{Au}_{30}\text{Ag}_{70}$ (at.%) was cold rolled, heat treated at 350 $^\circ\text{C}$ for one day and dealloyed in similar conditions as the rectangular blocks, followed by coarsening in acid. The resulting sample with weight $\sim 280 \text{ mg}$ was electrochemically cleaned and used for BET measurements for the determination of the exact value of the dimensionless constant in Eq. (4).

4. Results and discussion

A typical ordered structure of the double gyroid PS-b-P4VP(PDP)_x complex is shown in Fig. 2a. The BET surface area (S_{BET}) of a double gyroid structure with average ligament size $d \sim 68 \text{ nm}$ is $S_{\text{BET}} \sim 77 \text{ m}^2 \text{ g}^{-1}$ as determined from nitrogen adsorption. Taking as polymer bulk density $\rho \sim 1 \text{ g cm}^{-3}$ and knowing the ligament size $d \sim 68 \text{ nm}$, and the dimensionless constant ~ 5.8 , a specific surface area $S \sim 85 \text{ m}^2 \text{ g}^{-1}$ is obtained for double gyroid structures using Eq. (4). S_{BET} and S are comparable within a 10% tolerance.

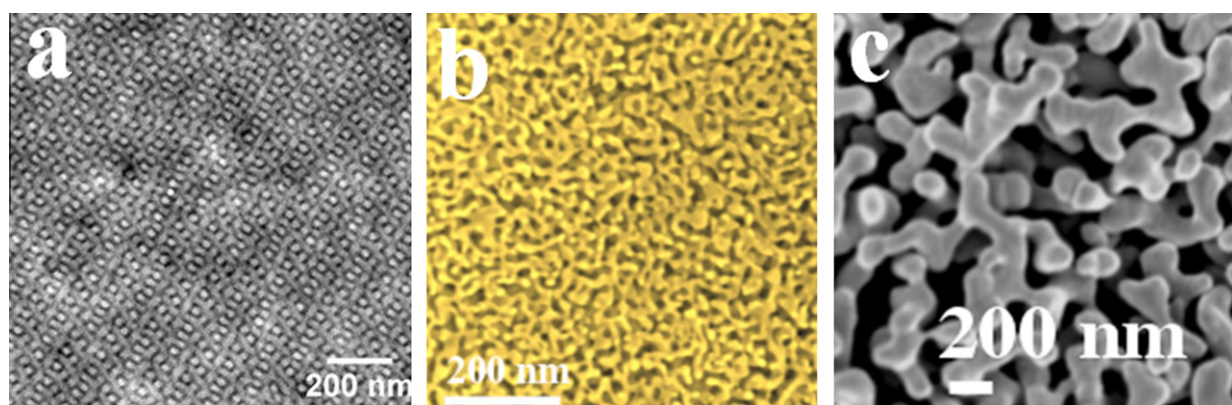


Fig. 2. Electron micrographs showing the microstructure of synthesized nanoporous materials. (a) Transmission electron micrograph of an ordered PS-b-P4VP(PDP)_x complex, a gyroid structure. This ordered morphology was made by block copolymer self-assembly. (b) Scanning electron micrograph of nanoporous gold made by the selective dissolution of silver from a gold-silver alloy. (c) Coarsened nanoporous gold ligaments after post-annealing treatments.

Charging/discharging curves of the seven planar solid gold electrodes were used to verify the dependence of the electrode surface area on the quantity of electric charge transferred during anion adsorption as shown in Fig. 3a. For each electrode 100 cycles were performed in order to verify its electrochemical stability, which is relevant for the investigation of the electrode surface area by charge adsorption. During the first cycles (approximately the first 10 cycles) the average charge transferred onto a planar gold electrode was in the range of $4\text{--}6\ \mu\text{C cm}^{-2}$. This corresponds to double layer capacitance values up to $\sim 32\ \mu\text{F cm}^{-2}$. These values are comparable to the $\sim 40\ \mu\text{F cm}^{-2}$ reported in literature during impedance measurement on non-oxidized planar gold surfaces [27,28].

As more cycles are performed, the quantity of charge transferred onto the planar gold electrodes decreases as displayed in Fig. 4a and stabilizes around a value of $\sim 1.5\ \mu\text{C cm}^{-2}$, usually after 20 cycles. In order to achieve reliable measurements of the electrode surface area, attention was paid to the stable cycles (i.e. $\sim 20\text{--}100$ cycles). It was observed that the larger the electrode surface area, the higher the charging/discharging current (see Fig. 3a). The variation of the average electric charge transferred during each cycle as a function of the electrode surface area is shown in Fig. 4b (for stable cycles). The average charge adsorbed onto a solid gold electrode (slope of the linear fit in Fig. 4b) was found to be $1.5\ \mu\text{C cm}^{-2}$. It is concluded that the quantity of electric charge transferred onto a solid gold electrode is linearly proportional to the electrode surface area. In the next section, this linear dependence will also be assumed to hold for nanoporous gold electrodes with unknown surface areas.

A scanning electron micrograph of the microstructure of a freshly dealloyed nanoporous gold sample is displayed in Fig. 2b. The average ligament size varies between 11 ± 3 and 29 ± 4 nm depending on the initial master alloy composition and the coarsening time in acid. Larger ligament sizes – namely 70 ± 20 and 100 ± 30 nm – were achieved

by post-annealing treatments. A typical structure of a thermally treated sample is shown in Fig. 2c. The large inhomogeneity in the ligament size of the two post-annealed samples (up to ± 30 nm) is due to the fact that the microstructure of these samples is not uniformly distributed: ligaments at the sample surface were observed to be larger than those in the bulk. This inhomogeneity in structure size was taken into account during electrochemical investigation of the surface areas of the two post-annealed samples.

The linear dependence on the adsorbent surface area of the charge electro-adsorbed onto a planar solid gold electrode was also applied to nanoporous gold electrodes. Fig. 3b displays charging/discharging curves of three out of eight nanoporous gold samples with different ligament sizes. As with planar solid electrodes, 100 cycles were performed for each of the eight nanoporous gold electrodes in order to take into account the electrochemical stability of the process. The charging/discharging current intensities were observed to increase with decreasing ligament size. This is in agreement with the behavior observed on planar solid gold electrodes, since small ligament sizes are associated with large surface areas.

The surface area of each nanoporous gold electrode was deduced for stable cycles ($\sim 20\text{--}100$ cycles) by comparing the electric charge adsorbed by each sample to that adsorbed by a planar solid gold electrode per unit surface area ($1.5\ \mu\text{C cm}^{-2}$) under similar conditions. Corresponding specific surface areas S were plotted as a function of ρd . As shown in Fig. 5, the electrochemical data fit well with the expression in Eq. (4). The value of the fitting constant was found to be $\sim 10 \pm 3$ for disordered nanoporous gold. These results are in good agreement with Eq. (4), which means that beside nanoporous materials with regular structures, Eq. (4) can be used to evaluate the specific surface area of disordered nanoporous materials as well. In contrast to the computed data (solid markers in Fig. 1e) which are all aligned on the corresponding solid curves, it can be seen that all the electrochemical data

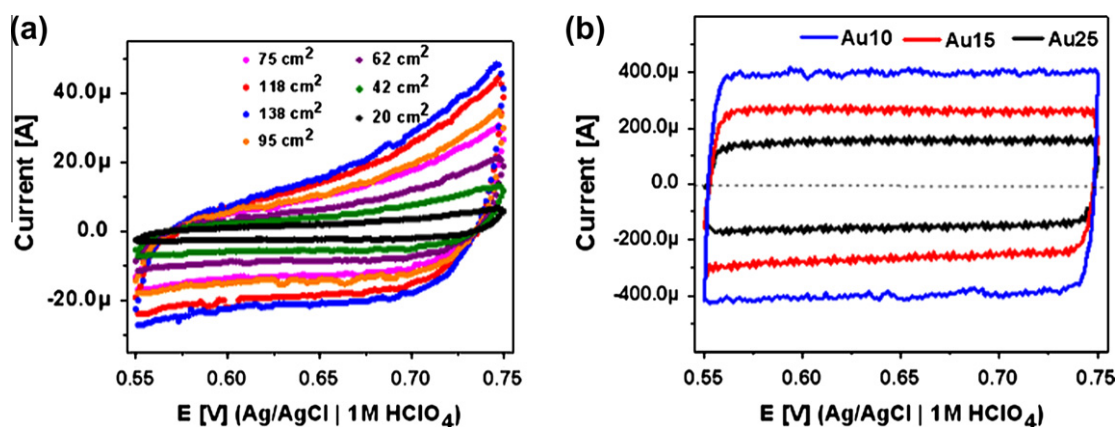


Fig. 3. Cyclic voltammograms of gold electrodes in the double layer charging regime. (a) Seven planar solid gold electrodes were used to verify the dependence of the quantity of electric charge transferred during anion adsorption on the electrode surface area. (b) Results of three of the eight investigated nanoporous gold samples with different ligament sizes. Charging/discharging current intensities were observed to increase as ligament size decreases.

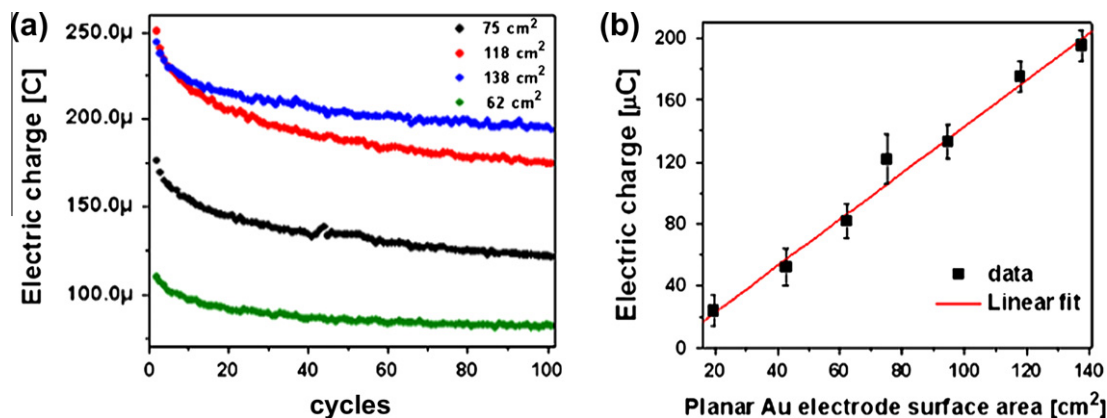


Fig. 4. (a) Electric charge transferred onto the planar gold electrodes (four of the seven electrodes) over 100 cycles. The quantity of charge transferred during the first cycles starts off large and decreases rapidly, stabilizing after 20 cycles. (b) Average charge adsorbed onto a solid gold electrode as a function of the electrode surface area. The quantity of electric charge increases with increasing electrode surface area.

(red markers in Fig. 5) are not precisely on the solid green line in Fig. 5. This has to do with the fact that the nanoporous gold samples do not have the same relative density. In spite of the fact that the material relative density is not explicitly taken into account in Eq. (4), this analytical model still gives good predictions (within the experimental error) of the specific surface area, for small variations in the relative density.

It can be seen in Fig. 5 that electrochemical data do not overlap with the BET data. A possible explanation might be the non-validity of the aforementioned assumption, according to which electric charge adsorbed onto a porous gold electrode per unit surface area was assumed to be equal to that adsorbed onto a planar solid gold electrode ($1.5 \mu\text{C cm}^{-2}$). It should also be noticed that due to polishing, the effective surface area of the planar solid electrodes might be higher than the surface areas used to evaluate the solid electrode charge density. Inaccuracies in the value of the solid gold electrode charge density will affect the value

of the fitting constant ($\sim 10 \pm 3$), but not the qualitative result, i.e. not the dependence of the specific surface areas S on ρd , as derived in Eq. (4). Another possible origin of the difference between electrochemical and BET data can be associated to systematic experimental errors. During electrochemical investigation of the specific surface area, the weight and the average ligament size of each nanoporous gold specimen are measured. Possible systematic errors introduced during these measurements might significantly affect the specific surface area values and subsequently the value of the fitting constant. Furthermore, to determine an adsorbent surface area, a monolayer coverage of the surface with adsorbates is appropriate. A drawback of the electrochemical method explored in this paper is that the precise nature of the coverage of the gold electrode surface by anions is not well-defined: charge transferred during electro-adsorption might involve a sub-, mono- or multilayer coverage. Sub- or multilayer coverage might give rise to under- or overestimated values for the surface

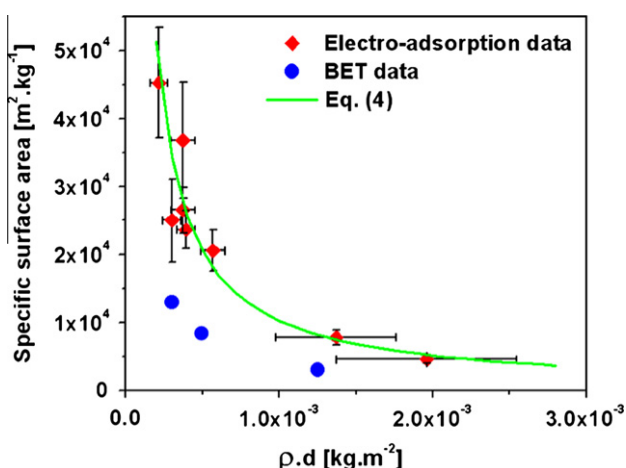


Fig. 5. Specific surface areas of nanoporous gold as a function of the ligament size. The red rhombus data (red markers) corresponds to the electrochemically measured specific surface areas. The green line is the prediction from Eq. (4) and the blue circles correspond to BET surface areas. The first two BET data sets (from the left) are taken from literature (see Refs. [2,8]). (For interpretation of the references to colour in this figure legend, the reader is referred to the web version of this article.)

areas and subsequently for the fitting constant. Therefore the value of the dimensionless constant in Eq. (3) was deduced from BET measurements.

Fig. 6a displays the nitrogen adsorption/desorption isotherm curve performed on a 256.6 mg nanoporous gold sample with average ligament size ~ 65 nm. This curve is characterized by a hysteresis loop associated with capillary condensation at high relative pressure. The curve corresponds to the Type IV isotherms according to the IUPAC classification, with respect to gas adsorption in macropores (widths >50 nm) [29]. The initial part (low relative pressures) of the isotherm in Fig. 6a is associated to the monolayer adsorption; the quantity of nitrogen gas adsorbed in

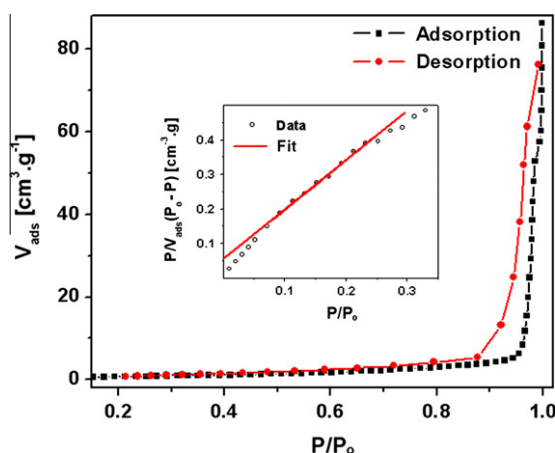


Fig. 6. (a) Nitrogen adsorption/desorption isotherm curve performed on a nanoporous gold sample with average ligament size ~ 65 nm. The initial part of the isotherm curve at low relative pressures corresponds to monolayer adsorption. (b) The quantity of nitrogen gas adsorbed at low relative pressures is used by the BET method to determine the specific surface area. The BET surface area and constant were deduced from the slope and offset of the linear part of the nitrogen adsorption isotherm.

that range is used for the evaluation of the specific surface area according to the BET method. The BET surface area ($S_{\text{BET}} \sim 3 \text{ m}^2 \text{ g}^{-1}$) and constant ($C_{\text{BET}} \sim 28$) were deduced from the slope ($1.446 \pm 0.034 \text{ cm}^{-3} \text{ g}$) and offset ($0.053 \pm 0.006 \text{ cm}^{-3} \text{ g}$) of the linear part of the nitrogen adsorption isotherm ($0.05 < p/p^0 < 0.35$) as displayed in Fig. 6b [12–14].

The optimal value of the constant in Eq. (4) for disordered nanoporous materials was found to be ~ 3.7 . This constant was determined from the above measured BET surface area ($S_{\text{BET}} \sim 3 \text{ m}^2 \text{ g}^{-1}$ and $d \sim 65$ nm), in combination with literature values for BET surface areas of nanoporous gold: in Ref. [8], $S_{\text{BET}} \sim 10\text{--}15 \text{ m}^2 \text{ g}^{-1}$ for $d \sim 10\text{--}20$ nm and in Ref. [2] $S_{\text{BET}} \sim 7 \text{ m}^2 \text{ g}^{-1}$ for $d \sim 20\text{--}30$ nm. The three BET data (experimental and literature) are displayed by the blue dots in Fig. 5. These values are lower than the electrochemical data, meaning that surface areas evaluated from anions adsorption were overestimated.

The values of the dimensionless constant in Eq. (4) are summarized in Table 1 for investigated nanoporous structures. Using this dimensionless constant, the material solid bulk density and feature size (ligament or pore size), one can efficiently evaluate the corresponding specific surface area.

5. Conclusion

An analytic expression is proposed for the calculation of the specific surface area of arbitrary nanoporous materials. Specific surface areas of several types of nanoporous materials were investigated. The values of the specific surface areas predicted by the proposed expression are comparable to experimental values. The proposed analytical model could be a useful tool for an efficient evaluation of the specific surface area of nanoporous materials having comparable ligament and pore sizes, since it only requires knowledge of the material solid bulk density and its average ligament size.

Acknowledgements

The authors are grateful to The Netherlands Organization for Scientific Research (NWO-The Hague, Mozaïek 2008 BOO Dossierrn: 017.005.026) and the Zernike Institute for Advanced Materials for financial support. The authors thank S.S.R. Saane for the discussions.

Appendix A. Dimensional analysis

The starting point is the specific surface area in Eq. (2), $S = f(\rho^*, d)$ that can also be written as:

$$S = \text{const}^*(d)^\alpha (\rho^*)^\beta \quad (\text{A1})$$

The corresponding dimensional equation is given by:

$$\left(\frac{\text{m}^2}{\text{kg}}\right) = C^*(\text{m})^\alpha \left(\frac{\text{kg}}{\text{m}^3}\right)^\beta \quad (\text{A2})$$

This is reduced to the linear system:

$$\begin{cases} \alpha - 3\beta = 2 \\ \beta = -1 \end{cases} \quad (\text{A3})$$

the solution of which is:

$$(\alpha, \beta) = (-1, -1) \quad (\text{A4})$$

Eq. (3) can be deduced using the expressions in (A1) and (A4).

Appendix B. Nanoporous material with cylindrical pores

The objective is to confirm, with an analytical approach, the validity of Eq. (3). For simplicity a cubic bulk porous material with cylindrical pores is considered. We define the following material parameters:

- L : size of the cube
- d : cylinder diameter
- n : number of cylinders in the cube
- ρ : solid density of the material
- ρ^* : density of the porous cube
- ρ_r : relative density of the porous cube

The porous density of the cube and its volume can be written as follows:

$$\rho^* = \rho_r \rho \quad (\text{A5})$$

$$V = L^3 \quad (\text{A6})$$

It is assumed that n is large enough so that cylinders falling out of cube faces (e.g. half cylinders) can be neglected. The number of cylinders n can be written as a function of the ligament diameter d . To this end, we make use of the relative density. Assuming for simplicity that the cylinders (pores) are all oriented in the same direction, e.g. in the vertical direction, the upper (solid) surface of the cube $A_{cube,up}$ can be written as:

$$A_{cube,up} = \rho_r L^2 \quad (\text{A7})$$

The corresponding (open) surface of the cylinders $A_{cyl,up}$ is given by:

$$A_{cyl,up} = L^2 - \rho_r L^2 \quad (\text{A8})$$

The upper surface of one cylinder as a function of the cylinder diameter d is known:

$$A_{1cyl,up} = \frac{\pi d^2}{4} \quad (\text{A9})$$

whereas the upper surface of one cylinder can also be written as a function of the number of cylinders n , by dividing the expression in (A8) by n :

$$A_{1cyl,up} = \frac{L^2(1 - \rho_r)}{n} \quad (\text{A10})$$

By comparing (A9) and (A10) the parameters d and n can be deduced as follows:

$$d = \sqrt{\frac{4L^2(1 - \rho_r)}{\pi n}} \quad (\text{A11})$$

$$n = \frac{4L^2(1 - \rho_r)}{\pi d^2} \quad (\text{A12})$$

The solid surface of one cylinder, i.e. a cylinder side $A_{1cyl,side}$, is given by:

$$A_{1cyl,side} = \pi d L \quad (\text{A13})$$

By replacing d in (A13) by the corresponding expression from (A11) one can rewrite (A13) as follows:

$$A_{1cyl,side} = L^2 \sqrt{\frac{4\pi(1 - \rho_r)}{n}} \quad (\text{A14})$$

The total surface of all cylinder sides $A_{cyl,side}$ is the surface of one cylinder side $A_{1cyl,side}$ multiplied by the number of cylinders n :

$$A_{cyl,side} = n A_{1cyl,side} \quad (\text{A15})$$

By replacing $A_{1cyl,side}$ in Eq. (A15) by the expression in Eqs. (A14) and (A15) can be rewritten as follows:

$$A_{cyl,side} = L^2 \sqrt{4\pi n(1 - \rho_r)} \quad (\text{A16})$$

Finally, by replacing n in Eq. (A16) by the corresponding expression from Eqs. (A12) and (A16) is simplified to:

$$A_{cyl,side} = \frac{4L^3(1 - \rho_r)}{d} \quad (\text{A17})$$

Eq. (A17) can further be simplified by replacing L^3 by V :

$$A_{cyl,side} = \frac{4V(1 - \rho_r)}{d} \quad (\text{A18})$$

The total internal surface area of the cube $A_{total,cube}$ corresponds to the surface area of all cylinder sides:

$$A_{total,cube} = A_{cyl,side} = \frac{4V(1 - \rho_r)}{d} \quad (\text{A19})$$

The mass m of the cube is given by:

$$m = \rho^* \cdot V \quad (\text{A20})$$

The density ρ^* of the cube in Eq. (A20) can be replaced by solid density of the material using Eq. (A5):

$$m = \rho_r \rho V \quad (\text{A21})$$

The specific surface area of the cube is obtained by dividing the expression in Eq. (A19) by the mass (m) of the cube as given in (A21):

$$S_{cube} = \frac{4(1 - \rho_r)}{\rho_r \rho d} \quad (\text{A22})$$

By replacing $\rho_r \cdot \rho$ by ρ^* Eq. (A22) becomes:

$$S_{cube} = \frac{4(1 - \rho_r)}{\rho^* d} \quad (\text{A23})$$

By replacing $(1 - \rho_r)$ by the porosity ϕ , Eq. (A23) becomes:

$$S_{cube} = \frac{4\phi}{\rho^* \cdot d} \quad (\text{A24})$$

The factor (4ϕ) in Eq. (A24) represents the dimensionless constant mentioned in Eq. (3), which means that Eq. (A24) can be rewritten in the form:

$$S_{cube} = \frac{C^*}{\rho^* \cdot d} \quad (\text{A25})$$

i.e. equivalent to Eq. (3) as was the objective of this Appendix.

References

- [1] Wittstock A, Zielasek V, Biener J, Friend CM, Bäumer M. *Science* 2010;327:319.
- [2] Nagle LC, Rohan JF. *Int J Hydr Energy*; 2010. doi:10.1016/j.ijhydene.2010.09.077.
- [3] Xu C, Xu X, Su J, Ding Y. *J Catal* 2007;252:243.
- [4] Lang XY, Yuan HT, Iwasa Y, Chen MW. *Scripta Mater*; 2011. doi:10.1016/j.scriptamat.2011.01.038.
- [5] Liu H, Zhu G. *J Power Sources* 2007;171:1054.
- [6] Weissmüller J, Viswanath RN, Kramer D, Zimmer P, Würschum R, Gleiter H. *Science* 2003;300:312.
- [7] Jin HJ, Wang XL, Parida S, Wang K, Seo M, Weissmüller J. *Nano Lett* 2010;10:187.
- [8] Biener J, Wittstock A, Zepeda-Ruiz LA, Biener MM, Zielasek V, Kramer D, et al. *Nature Mater* 2009;8:47.
- [9] Jin HJ, Weissmüller J. *Adv Eng Mater* 2010;12:714.
- [10] Brunauer S, Emmett PH, Teller E. *J Am Chem Soc* 1938;60:309.
- [11] Brunauer S, Deming LS, Deming WE, Teller E. *J Am Chem Soc* 1940;62:1723.
- [12] Gregg SH, Sing KS. *Adsorption surface area and porosity*. New York: Academic Press; 1967.
- [13] Sing K, Everett D, Haul R, Moscou L, Perolti R, Rouquerol J, et al. *Pure Appl Chem* 1985;57:603.
- [14] Rouquerol F, Rouquerol J, Sing K. *Adsorption by powders and porous solids: principles, methodology and applications*. London: Academic Press; 1999.
- [15] Detsi E, Van de Schootbrugge M, Punzhin S, Onck PR, De Hosson JTM. *Scripta Mater* 2011;64:319.
- [16] Wang J, Duan HL, Huang ZP, Karihaloo BL. *Proc R Soc* 2006;A462:1355.
- [17] Gibson LJ, Ashby MF. *Cellular solids: structure and properties*. 2nd ed. Cambridge: Cambridge University Press; 1997.
- [18] Burke LD, Nugent PF. *Gold Bull* 1997;30:43.
- [19] Conway BE. *Prog Surf Sci* 1995;49:331.
- [20] Vukovic I, Punzhin S, Vukovic Z, Onck P, De Hosson JTM, ten Brinke G, et al. *ACS Nano* 2011;5:6339.
- [21] Ikkala O, Ten Brinke G. *Science* 2002;295:2407.
- [22] Mäki-Ontto R, De Moel K, De Odorico W, Ruokolainen J, Stamm M, Ten Brinke G, et al. *Adv Mater* 2001;13:117.
- [23] Valkama S, Ruotsalainen T, Nykänen A, Laiho A, Kosonen H, Ten Brinke G, et al. *Macromolecules* 2006;39:9327.
- [24] Gobius du Sart G, Vuković I, Vuković Z, Polushkin E, Hiekkataipale P, Ruokolainen J, et al. *Macromol Rapid Commun* 2011;32:366.
- [25] Erlebacher J, Aziz MJ, Karma A, Dimitrov N, Sieradzki K. *Nature* 2001;410:450.
- [26] Erlebacher J, Sieradzki K. *Scripta Mater* 2003;49:991.
- [27] Jin HJ, Parida S, Kramer D, Weissmüller J. *Surf Sci* 2008;602:3588.
- [28] Germain PS, Pell WG, Conway BE. *Electrochim Acta* 2004;49:1775.
- [29] Klobes P, Meyer K, Munro RG. *Spec Publ* 2006; 960:17 [Natl. Inst. Stand. Technol. Washington].